Microstructured Water-Based Broadband Terahertz Pyramidal Absorber

Kalliopi Spanidou, *Student Member, IEEE*, Daniel Headland, *Member, IEEE*, Sharath Sriram, Itziar Maestrojuán Biurrun, and Guillermo Carpintero, *Senior Member, IEEE*

***Abstract*—The presence of multipath effects in terahertz wireless links degrades signal quality, making absorbers a critical component of 5G/6G wireless systems. Here, we leverage the innately high loss of liquid water, combined with the microscale precision of UV-cured resin-based micro 3-D printing, to realize a viable pyramidal absorber for terahertz waves. Both simulation and experimental results confirm near-unity absorption, achieving over 99% in the 75–190 GHz range and 99.99% over 190–500 GHz. Furthermore, simulations show that the absorber maintains high performance up to 1000 GHz, with absorption exceeding 99.999%. These results demonstrate potential for future micro 3-D-printed resin-based absorbers that can be readily tailored to serve in communication, sensing, and radar applications, thanks to their microscale size, cost-effectiveness, and adaptability to broadband terahertz wireless systems.**

***Index Terms*—Antenna shielding, broadband communication, electromagnetic absorbers, micro 3-D printing, resin, terahertz radiation.**

I. Introduction

As WIRELESS technology rapidly advances, expanding to higher frequencies beyond the microwave range is increasingly motivated by the needs of 5G/6G communication networks [1], [2], [3], and a growing number of applications in sensing [4], imaging [5], [6], and radar testing [7]. The capabilities offered by such systems are enriched in various aspects, such as high bandwidth and high resolution, by the use of terahertz waves. However, there is also a growing need for reliable signal detection and high transmission purity, and this presents significant challenges in the presence of multipath. While the microwave range offers signal-processing techniques to mitigate the undesired effects of multipath [8], or even exploit them for signal diversity in MIMO systems [9], this approach is infeasible for the high-frequency and large channel bandwidths associated with terahertz wireless technology. For this reason, it is essential to mitigate multipath effects and signal degradation at the physical level, by ensuring a single flight in a line-of-sight between the source and the detector. Thus, high-performance absorbers are a critical necessity.

Traditionally, standard microwave-range pyramidal absorbers have used ferrite [10] and polymer composites, such as polyurethane [11], [12] and carbon-loaded urethane absorbers achieving reflectivity of −55 dB up to 110 GHz [13]. However, the dielectric properties of such materials are ill-suited for short wavelengths, and fabricating high-aspect-ratio pyramid structures at the microscale with these methods has proven challenging. Only a few examples made from carbon-loaded polypropylene provided in flat-panel tiles exhibit high performance, achieving losses of −60 dB up to 650 GHz [14]. Highly specialized terahertz materials, such as TK RAM, excel in controlled environments; however, the use of injection molding imposes inherent limitations when adapting to more intricate geometries. A potential issue arising in the polymer matrix is its inherent fragility due to carbon powder impregnation, which can undermine its structural integrity [15]. Consequently, the constrained design flexibility and precision at the microscale imposed by the manufacturing process pose significant challenges to effective deployment in real-world environments.

Given the difficulties associated with adapting classical microwave-range absorbers to the microscale, terahertz absorbers have seen significant design innovations, especially in the form of planar metamaterials. The fundamental operating principle of these metamaterials lies in the collective interaction of an array of tailored meta-atoms with terahertz waves designed to resonate at certain frequencies, offering efficient control over electromagnetic waves [16], [17], [18]. However, the use of resonance effects limits the bandwidth, and so broadband functionality often depends on complex stacked multiresonant layouts that are difficult to fabricate [17]. One more favorable approach to increase bandwidth focuses on dielectric materials combined with graphene to increase absorption by introducing magnetic loss [19], [20],

Received 26 January 2025; revised 31 March 2025 and 23 May 2025; accepted 7 June 2025. This work was supported in part by the Horizon 2020 Excellent Science–Marie Sklodowska-Curie Actions (TERAOPTICS Project) under Grant 956857, in part by the Smart Networks and Services Joint Undertaking (SNS JU) under the European Union's Horizon Europe Research and Innovation Programme (TERA6G Project) under Grant 101096949, in part by the Universidad Carlos III de Madrid and the European Union's Horizon 2020 Research and Innovation Programme Marie Sklodowska-Curie (CONEX-Plus) under Grant 801538, in part by the European Union through Horizon Europe Framework Programme (POLYNICES Project) under Grant 101070549, and in part by APC: Universidad Carlos III de Madrid (Agreement CRUE-Madroño 2025). *(Corresponding author: Kalliopi Spanidou.)*

Kalliopi Spanidou, Daniel Headland, and Guillermo Carpintero are with the Optoelectronics and Laser Technology Group, Department of Electronics Technology, Universidad Carlos III de Madrid, 28911 Madrid, Spain (e-mail: kspanido@ing.uc3m.es; dheadlan@ing.uc3m.es; guiller@ing.uc3m.es).

Sharath Sriram is with the Functional Materials and Microsystems Research Group and the ARC Centre of Excellence for Meta-Optical Systems, RMIT University, Melbourne, VIC 3001, Australia.

Itziar Maestrojuán Biurrun is with Anteral S.L., 31006 Pamplona, Spain.

Data is available on-line at https://doi.org/10.5281/zenodo.15691812.

Digital Object Identifier 10.1109/TMTT.2025.3580219

[21], [22]. Graphene sheets are known to contribute significant ohmic loss, and so hosting flakes of graphene in a polymer matrix has enabled terahertz absorbers up to 600 GHz [22]. However, their limited intrinsic absorption, coupled with difficulties in precisely controlling the material structure, constrains their applicability in high-frequency wireless systems. These limitations highlight the necessity for advanced fabrication approaches that enable greater design diversity, including higher aspect ratios, enhanced electromagnetic properties, and adaptability for broadband performance.

Advances in micromanufacture have enabled the realization of intricate nonplanar geometries using silicon, due to its compatibility with techniques such as deep reactive ion etching. Owing to the strong conduction losses of doped silicon, shallow-etched 3-D structures can achieve high absorption by exploiting band-edge resonances, though their performance remains inherently narrowband [23]. Moreover, geometrically intricate structures, such as arrays of cross-shaped [24], [25] and inverted pyramidal [26] structures, show exceptionally broad bandwidth at terahertz up to far-infrared due to combined resonance effects of the plasmonic cavities. Another example is grating-based multilayer structures, which achieve similar broadband performance by leveraging multiorder diffraction effects [27]. However, broadband absorption is generally between 10 and 20 dB, primarily limited by the aspect-ratio constraints of deep etch fabrication techniques used to realize the microstructured topologies. This level of absorption performance falls below the typical standards required in effective electromagnetic shielding applications. Alternative microfabrication strategies are therefore required to enhance the aspect ratio of 3-D microstructures.

UV-cured resin-based micro 3-D printing offers design freedom in creating complex, high-aspect-ratio microscale structures. This technique has been used to fabricate resin-based microstructured absorbers, including multiresonant metal composites [28], arrays of cross-shaped resonators with different lengths [29], and classical pyramidal absorbers that exploit the intrinsic dielectric loss of the resin [30]. However, the intrinsic loss of the 3-D-printed resin is limited. This is why, although the latter cited work does indeed achieve high absorption of 50 dB above 250 GHz, this demands a taper length of $>15\lambda_0$, posing a significant barrier to practical deployment. Not only that, loss also reduces to <10 dB below 85 GHz due to diminishing intrinsic absorption of the resin at lower frequencies. It would therefore be beneficial to combine the structural versatility of UV-cured resin micro 3-D printing with the strong intrinsic absorption of a truly high-loss material.

One of the most notoriously lossy substances in the mm-wave and terahertz ranges is ordinary liquid water, which presents a significant problem in signal degradation for communication links in humid conditions [31]. Thus, it is widely regarded as a major obstacle to the adoption of wireless terahertz technologies. However, this has not wholly impeded the deployment of this material to construct terahertz devices as, perhaps surprisingly, terahertz waves have previously been generated by exploiting the high nonlinearity of liquid water by means of intense laser pulses [32]. Researchers have since leveraged water's high dielectric loss to develop high-performance absorbers across the full microwave regime [33], [34], [35], [36], and extending to the mm-wave regime using mushroom-shaped [37] and ring resonators [38]. Advanced fabrication techniques have raised operational frequency up to 100 GHz [39], [40], and plexiglass-based structures have demonstrated single-frequency absorption of 60 dB at 240 GHz [41]. While these techniques offer high absorption for particular frequency ranges, their design complexity increases while expanding to broader operation ranges.

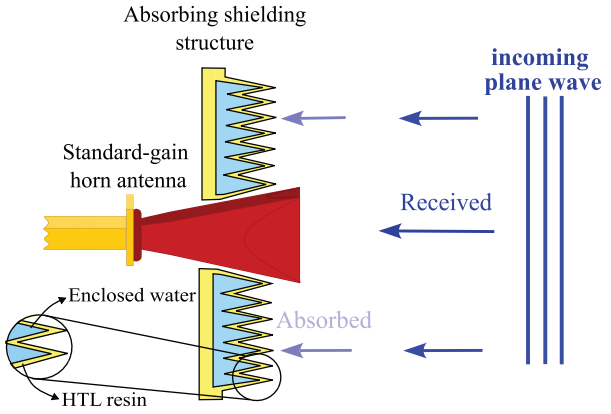

Fig. 1. Schematic illustration of the proposed water-based pyramid absorber used as a shielding structure of a terahertz horn antenna. The design features the relief structure with the liquid water enclosed and the HTL resin-based pyramid arrays under normal incidence.

In this work, we present a broadband pyramid absorber for mm-wave and terahertz frequencies composed of ordinary liquid water. An illustration of the proposed water-based pyramid absorber designed for horn-antenna shielding is depicted in Fig. 1. This is enabled by a UV-cured resin 3-D-printed hollow pyramid-array relief structure, which simultaneously encloses a reservoir of liquid water while imposing the desired microscale pyramid shape upon it. Micro 3-D-printed structures that enclose lossy liquid metal have previously enabled terahertz absorbers, albeit with notable dips in absorption below 90% over the stated operation bandwidth [42]. Alternatively, the hollow cavity could be filled with liquid crystal to enable tunability under high bias fields [43]. However, this approach is not required in this case, since broadband performance precludes the need for frequency tunability. Our absorber demonstrates high absorption performance across a broad bandwidth, achieving measured absorption of 99% over 75–110 GHz and 99.99% over 140–500 GHz. The high absorption levels primarily result from the significant dielectric loss of water at low frequencies and resin at high frequencies, combined with the progressive matching effect that arises due to the microstructured pyramid geometry. In addition, simulations up to 1000 GHz confirm high-frequency operation, achieving high absorption of 99.999%. Therefore, the proposed absorber is well-suited for mitigating multipath effects in wireless links, enhancing electromagnetic shielding of antenna test equipment, and suppressing undesired leakage signals.

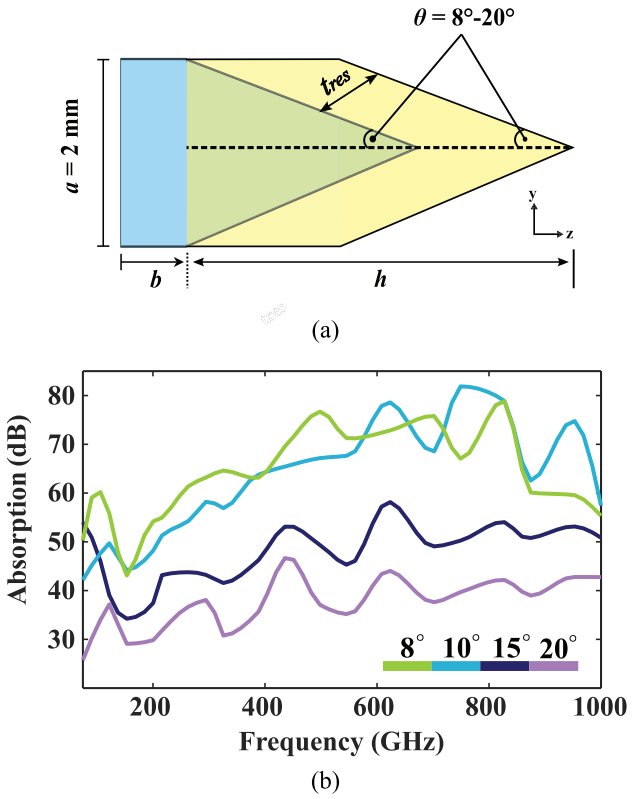

Fig. 2. (a) Illustration of the unit cell of the proposed terahertz absorber in cross-sectional view with the given detailed dimensions. (b) Absorption spectra of the proposed water-based absorber under normal incidence for different slope angles ranging from 8° to 20°, obtained from full-wave simulations.

II. Design Concept and Analysis

The unit-cell geometry of the proposed relief absorbing structure is illustrated in Fig. 2(a). In this design, two key principles are crucial for the absorbing structure's operation: the pyramidal taper that yields progressive impedance matching to free space, and the use of liquid water as the lossy medium, with $\epsilon = 6$ and $\tan\delta = 1.01$ at 300 GHz, with broadband dispersive properties accurately described by the Debye formula [44]. The absorber consists of a relief structure formed by resin-based hollow pyramid arrays to enclose the liquid water. The overall pyramid design is parameterized in terms of period a, base thickness b, taper angle θ, and wall thickness of the resin, t_{res}.

The performance of the absorber is analyzed using full-wave simulations implemented with the commercially available software package CST Studio Suite. The proposed structure is designed to operate within the 75–>1000-GHz range, while the upper limit for the experimental validation is set to 500 GHz by to the available instrumentation, which will be discussed in Section III. The relative permittivity and loss tangent of the resin substrate are equal to $\epsilon = 3$ and $\tan\delta = 0.03$ at 300 GHz [28]. The pyramidal array has a 2-mm period, designed to interact efficiently with terahertz radiation in this frequency range, maintaining consistency with prior pyramid-absorber studies and enabling a fair and direct comparison [15], [30]. This value of a remains fixed during the analysis process. In addition, the thickness of the back layer is set to $b = 0$ mm for these simulations, to obtain a conservative estimate of performance, although it is noted that higher absorption can be achieved if it is extended. The resin wall thickness is 500 μm, although according to additional simulations (not shown), the specific value has minimal impact on the overall performance of the absorber. This is because the progressive matching operation of the pyramid geometry is primarily dependent on the slope angle of the pyramidal tip, which is independent of small variations in wall thickness.

The optimization process is a careful balance between electromagnetic performance and practical fabrication viability. In simulations, perfect electrical boundaries are applied to the back wall to establish a lower bound of absorption. A single Floquet port is set at $z_{\max}$, and unit-cell boundaries are set along the x- and y-axis directions. An incident terahertz beam is impinged on the unit-cell structure and propagates along the z-axis. The overall simulated absorption performance accounts for the possibility of nonspecular reflection due to diffraction effects by evaluating the total power delivered from the exciting Floquet port to the model, as opposed to the return loss in a given Floquet mode.

The absorption characteristics of four different taper angles are simulated, and the results are presented in Fig. 2(b). It can be seen that steep angles are favored as they are associated with superior matching and absorption. However, this results in taller pyramids, compromising compactness and manufacturability. In contrast, wider angles are expected to limit performance at high frequencies. The chosen slope range from 8° to 20° allows for a parameter space that spans between shallow pyramid designs [26] and more optimistic designs with extreme slope angles [30]. Fortunately, given the manufacturing flexibility of the resin micro 3-D printing, we have significant freedom to select the desired slope angle. As can be seen, all the designs show absorption levels above 30 dB, equivalent to over 99.9% and reaching beyond 50 dB, i.e., 99.999%, particularly for the more severe slope angles at higher frequencies. However, such steep angles will be avoided due to the potential challenges related to water ingress in practice. In addition, 20° angle exhibits good performance, starting at around 30 dB and gradually reaching 40 dB, i.e., 99.99%, from 400 GHz and beyond. The 15° angle was therefore selected as an optimal balance for this design in terms of high performance and ease of fabrication. Across the entire frequency range, the structure achieves sufficient absorption with levels ranging from 35 to 40 dB above >150 GHz to 50 dB at higher frequencies, particularly in the range above 400 GHz.

To provide additional insight, a detailed theoretical analysis of the equivalent circuit model is conducted to evaluate the performance of the chosen design. The equivalent circuit model of the proposed terahertz absorber with a selected 15° slope angle is derived, as shown in Fig. 3(a). The analysis combines effective medium theory with transmission line modeling, and hence omits diffraction and scattering phenomena from consideration. This allows us to consider the progressive matching operation of the tapered pyramid itself, and

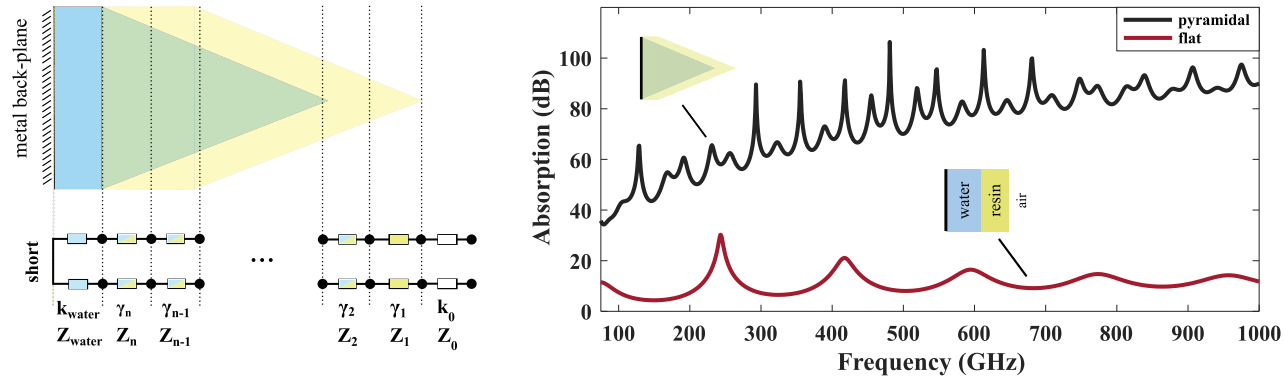

Fig. 3. (a) Equivalent circuit model of the proposed water-baser absorber. (b) Absorption spectra of the absorber with 15° slope angle and the flat absorber, both derived from the equivalent circuit model.

thereby gauge the impact of the aforementioned nonspecular reflection effects that are modeled in the full-wave simulation via cross-comparison. The structure is approximated as a set of series-connected subwavelength transmission lines, starting with a short-circuit representing the package's metal back-plane, as detailed in Section III. By dividing the structure into a series of n subwavelength slices of 10 μm, computing the effective medium properties of each, and then representing them with lengths of the transmission lines characterized by γ_c and Z_c, where $c = 1, 2, \ldots, n$. Using the generalized Maxwell Garnett formula for multicomponent mixtures in a host material [45], the complex effective permittivity ϵ_c can be computed directly by applying the following equation for mth inclusion:

$$\frac{\varepsilon_c - \varepsilon_h}{\varepsilon_c + 2\varepsilon_h} = \sum_{m=1}^{N} f_m \cdot \frac{\varepsilon_m - \varepsilon_h}{\varepsilon_m + 2\varepsilon_h} \tag{1}$$

where, in this case, the host material is resin, with a permittivity of ϵ_h, while water and air are the inclusions with permittivities ϵ_m and corresponding volume fractions f_m. Considering a homogeneous lossy medium, the complex propagation constant and impedance can be expressed as

$$\gamma_c = jk_0 \cdot \sqrt{\epsilon_c} \tag{2}$$

$$Z_c = \frac{Z_0}{\sqrt{\epsilon_c}} \tag{3}$$

where ϵ_c is the complex effective permittivity, and Z_0 is the impedance in free space [46]. Accordingly, the solutions from telegrapher's equations for a lossy transmission line are represented as an $ABCD$ two-port network, as

$$\begin{bmatrix} A_c & B_c \\ C_c & D_c \end{bmatrix} = \begin{bmatrix} \cosh(\gamma_c \cdot l) & Z_c \cdot \sinh(\gamma_c \cdot l) \\ \sinh(\gamma_c \cdot l) \cdot Z_c^{-1} & \cosh(\gamma_c \cdot l) \end{bmatrix}. \tag{4}$$

We approximate the short-circuited base with a finite impedance of $Z_{\text{short}} = 10^{-6}$ Ω, which results in a noninfinite C-parameter, i.e., $C_{\text{short}} = 1/Z_{\text{short}}$. The $ABCD$ matrix for each segment of the transmission line is then computed accordingly. It is, therefore, convenient to determine the overall performance of the absorber from deriving the cascaded $ABCD$ matrix for all the slices, and then convert it into S-parameters to find the S_{11} parameter for the entire frequency band [47]. The resultant absorption spectrum is depicted in Fig. 3(b), compared with the scenario featuring a flat geometry. These results show a substantial enhancement in absorption attributed to the presence of the pyramid structure, which effects a progressive impedance transition between free space and the absorbing medium. A similar behavior is observed from 100 GHz and above when compared with simulations, albeit with higher absorption. This outcome is expected, as the analytical model assumes wave propagation solely in the longitudinal direction, thereby neglecting secondary wave phenomena and resulting in higher loss. At the lower bound of the frequency range, however, the absorption levels deviate from the analytical model, with full-wave simulations predicting higher loss. This discrepancy arises from diffraction and scattering phenomena occurring within the high-refractive-index medium. In the latter, these effects result in wavelength compression and increased internal scattering, which collectively trap the energy and hinder its reradiation back into free space. These observations reveal inherent differences between the two methodological approaches, particularly in the physical phenomena they account for.

To elucidate the operation of the water-based pyramid absorber, Fig. 4(a)–(c) shows the loss distributions at frequencies of 100, 300, and 500 GHz, respectively, as derived from full-wave simulation. We concentrate on the 75–500-GHz frequency range, to maintain consistency with the measurement range addressed in Section III. As observed at the lower end of the frequency range, absorption is primarily concentrated toward the apex of the water pyramid, indicating that high performance can be achieved without requiring an extended reservoir. At higher frequencies, especially at 500 GHz, resin acts as a more lossy medium, and hence contributes a greater proportion of loss. To quantify this shift, we compare the relative loss in each material across the entire frequency range shown in Fig. 4(d). Specifically, above the crossover frequency of 350 GHz, the resin exhibits higher power loss, whereas water indicates a dominant role in the lower frequency band. This performance trend is well-aligned with previous reports

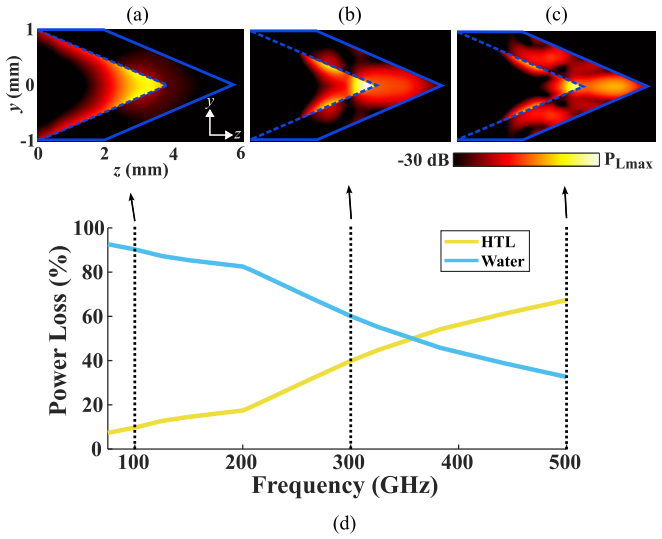

Fig. 4. Power absorption density distribution of the designed pyramidal relief structure with 15° slope angle at specific frequencies of interest (a) 100, (b) 300, and (c) 500 GHz, showing power absorption levels from −30 dB to $P_{L\max}$. (d) Simulated power loss for HTL and water as a function of frequency, with emphasis on the three selected frequencies.

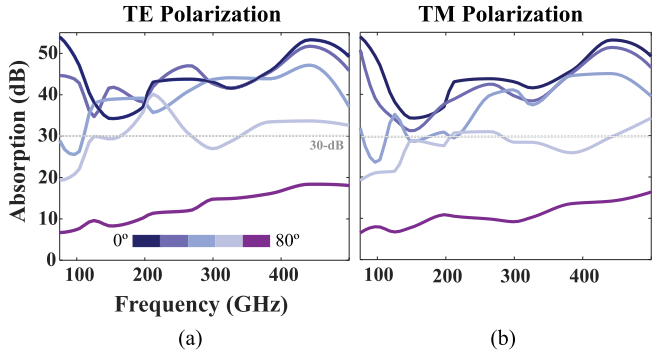

Fig. 5. Simulated absorption spectra at different incidence angles between 0° and 80° for (a) TE and (b) TM polarizations.

[30], in which an all-resin pyramid is able to achieve high absorption only at higher frequencies.

To further evaluate the capabilities of the proposed absorber, it is important to consider that normal incidence is not the sole possibility; the absorber's ability to sustain high absorption across various angles of incidence must also be verified. For this simulation, we are focusing on 15° slope representing the lower bound of performance up to 500 GHz, as a continuation of the study based on previous results. Fig. 5(a) and (b) depicts the absorption for TE and TM polarizations at various incidence angles ranging from 0° to 80° in 20° increments, respectively. Across the entire frequency range, the absorber maintains high absorption albeit with some performance degradation. Particularly, high absorption beyond 30 dB and broadband performance is shown under <20° angle of incidence for the entire range. For the incidence angle of 40°, a strong absorption of 30 dB is evident from 110 and 220 GHz up to 500 GHz for TE and TM polarizations, respectively. An additional increase to 40 dB is observed >250 GHz for TE polarization and >350 GHz for TM polarization. However, absorption becomes unsatisfactory at high incidence angles, such as grazing incidence at 80° angle. This is expected, since the pyramid is specifically designed to achieve progressive matching primarily along the z-axis. Future designs have the potential to significantly enhance absorption at oblique angles by corrugating the wall surfaces of the pyramid, as reported in [48], through the use of square-shaped subwavelength gratings. In principle, the use of micro 3-D printing opens the door to such advanced microstructures, to further optimize performance as needed.

III. Results and Discussion

The proposed water-based pyramidal absorber is fabricated to facilitate experimental characterization. To maintain a manageable scope, we select a single design as proof of concept for this purpose, for which we find that 15° angle allows efficient absorption in the range of 75–500 GHz. The height of the total absorbing tip measures 5.8 mm, with the resin layer thickness of 500 μm. This design effectively balances compactness, performance, fabrication, and assembly considerations.

A. Assembly Procedure

The designed terahertz absorber is fabricated by projection micro stereolithography (PμSL) technique using the S230 microArch resin 3-D printer from Boston Microfabrication.[1] A photograph of the relief structure is shown in Fig. 6(a), with a close-up microscope image of the pyramidal tips in Fig. 6(b). The PμSL technique features high printing resolution of 2-μm, making it ideal for microscale fast prototyping and fabrication. The use of UV light curing permits fine detail, fast printing speeds, and excellent material durability of the final printed parts [42]. The designed pyramid array spans 20 periods, covering a square area of 40 × 40 mm^2. A metal package is designed to enclose distilled water in the pyramidal relief structure during the experimental probing. A general-purpose syringe is used to fill each pyramidal cavity with the liquid.

To prevent water leakage, we apply petroleum jelly to the edges of the metal package avoiding the pyramidal cavities, prior to assembly to form a temporary hydraulic seal. This approach ensures a secure seal during the demonstration, although it may introduce slight variations in the homogeneity of the filling medium. One complication encountered during this assembly procedure is the formation of microbubbles at the tip of each pyramid when the water is added, caused by surface tension. To eliminate these bubbles, a needle is used to manually puncture and release them. In future iterations, this manual procedure could be replaced with a vacuum-environment-based assembly to wholly evacuate all the gases prior to assembly, thereby obviating the need for any sealant material.

[1]See Boston Microfabrication, S230 MicroArch Resin 3-D Printer, accessed November 10, 2024.

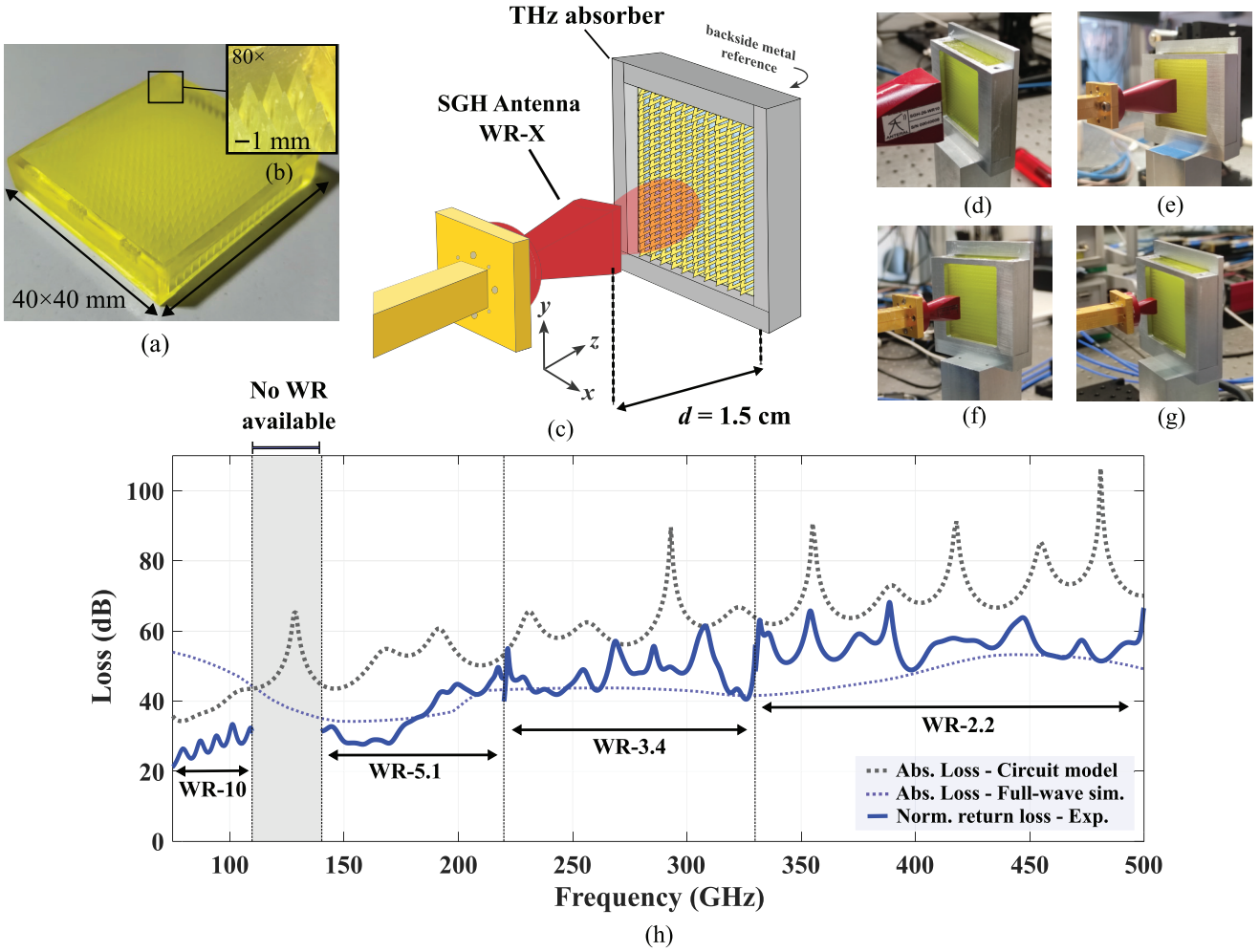

Fig. 6. (a) Photograph of the proposed pyramidal absorber. (b) Micrograph of the tips. (c) Illustration of the experimental setup for absorber characterization, including the hollow waveguide and the SGH antenna positioned 1.5 cm away from the absorber, which is enclosed in a metal package. Photographs of the individual tests are presented for (d) WR-10, (e) WR-5.1, (f) WR-3.4, and (g) WR-2.2 frequency bands. (h) Measured absorption levels across the entire frequency band, derived from normalized reflection (return loss) measurements, compared with simulated and theoretical results representing total absorption loss.

B. Experimental Validation

The absorption characteristics are evaluated by normalized return loss measurements. Fig. 6(c) illustrates the experimental setup used, and all the measurements are performed under the same conditions: normal incidence of the terahertz beam with a short standoff distance of ~1.5 cm. Measurements at oblique angles are not considered due to practical challenges, including inherent limitations associated with the available instrumentation, insufficient aperture size, and ambiguities regarding the appropriate longitudinal position of the normalization-reference plane at oblique angles owing to the absorber's nonplanar geometry and finite size. Nevertheless, this restriction does not compromise our confidence in the performance of the absorber, as normal incidence provides sufficient information to evaluate and demonstrate the core functionality of the proof-of-concept. Owing to its rotationally symmetrical geometry, no variation is anticipated with respect to the polarization angle of the incoming radiation at normal incidence. The flat backside of the metal package is used as a conductive mirror, to serve as a reference. In addition, the sample is situated on top of a rotation stage allowing us to obtain this reference directly by rotating it 180°.

To verify the absorption performance, a vector network analyzer is equipped with a range of frequency extension heads to cover from 75 to 500 GHz. Each individual band demands its own specific standard-gain horn (SGH) antenna, supplied by Anteral S.L. as shown in Fig. 6(d)–(g). We also note that there is a gap in frequencies between 110 and 140 GHz due to a lack of the appropriate instrumentation system for this range. Insertion loss is calculated as the discrepancy in measured $|S_{11}|$ between the absorber sample and the reference mirror. The acquired data are time-gated prior to normalization to isolate the response of the pyramid absorber. Specifically, Hann windowing is applied in the frequency domain to reduce spectral leakage, and Hamming windowing to the time-domain signal to isolate the response of a single flight from the antenna to the sample and back.

The measured results given in Fig. 6(h) show that absorption progressively increases with frequency. Starting from 20 dB

TABLE I
COMPARISON OF BROADBAND ABSORBERS ABOVE 100 GHZ

Absorber type	Dimensionality	Thickness (μm)	Material	Absorption >10 dB (GHz)	Absorption >40 dB (GHz)	Ease of fabrication	Fragile
Pyramid [14], [15], [50]	3-D	7500	Carbon-loaded polypropylene	75 – 110, 140 – 180, < 200 – 650	75 – 110, 140 – 180, < 200 – 650 *	Medium	Yes
Photonic-crystal slab [23]	2.5-D	200	Si	275 – 325	–	High	Yes
Cross-shaped [24]	2.5-D	265	Si	670 – 1780	~1490	High	Yes
Grating [27] †	3-D	500	Si	< 200 – 2500	~2083	High	Yes
Film [22]	2-D	600	Graphene + PTFE	210 – 600	–	Low	No
Hollow cross-shaped [25] †	3-D	400	Si + Air	600 – 800, 1100 – 1750, < 2100 – 2500	~2500	High	Yes
Inverted pyramids [26] †	3-D	250	Si	1250 – 20000	–	High	Yes
Cross-shaped [29] †	3-D	25	Resin + Au	659 – 802	–	High	Yes
Pagoda-like [28] †	3-D	39.2	Resin + Au	< 450 – 1600	~900	Medium	Yes
Pyramid [30]	3-D	26200	Resin	< 85 – 155, < 225 – 325	~215 – >325	High	No
Fabry-Perot cavities [42] †	3-D	2250	Resin + Liquid metal	260 – 315, 360 – 580	~385, ~400, ~450, ~530	Low	No
Pyramid (this work)	**3-D**	**5800**	**Resin + Liquid water**	**< 75 – > 500**	**190 – > 500**	**High**	**No**

* Experimental results report attenuation for individual frequencies for the 200–600 GHz range [14], [15], [50].

† Values were approximated from the provided absorption plots in linear scale, as they are not explicitly reported in dB scale in the source material.

at 75 GHz, corresponding to 99% absorption, the absorption increases to >40 dB from 190 GHz up to frequencies above 500 GHz, achieving 99.99% absorption. It can be seen that both the measured and simulated results show broad agreement, very strong terahertz absorption in broadband, and consistent trends with respect to frequency. Specifically, the experimental results show that absorption reaches approximately 30 dB around 170 GHz, and then exceeds 40 dB as it enters the WR-3.4 waveguide range and continues to increase over 50 dB within the WR-2.2 range. However, there are notable discrepancies in the specific reported value of loss, particularly in the WR-10 band. According to additional parametric perturbation analysis using the full-wave tool (not shown), this cannot be ascribed to physical tolerances of manufacture. The differences between the two models have already been discussed in detail in Section II. That said, both the modeling techniques use an infinite-sized array, which is excited by a plane-wave of infinite extent. On the other hand, the prototype of the absorber is composed of 20×20 periods, is enclosed within a package, and is illuminated with a finite-sized SGH antenna. Moreover, the theoretical models are capable of directly evaluating absorption loss, whereas the experiment probes specular return loss in the case of normal incidence. Another contributing factor is the practical limitation posed by the antenna size, which is approximately the same size as the array's aperture enclosed within the metallic package shown in Fig. 6(d). This results in reflections from the metal borders that cannot be removed from the response via time-gating. Overall, while these inherent differences in modeling and measurement preclude exact correspondence, they are all in agreement in the sense that they show high absorption across a broad operation bandwidth, and hence confirm the effectiveness of the design. The proposed absorber exhibits absorption above 20 dB, corresponding to over 99% absorption, for the entire frequency band, marking a significant improvement compared with the results reported in the literature [28], [30], [42].

A detailed comparison of the existing state-of-the-art broadband absorbers operating above 100 GHz is presented in Table I. These absorbers, which use various materials and fabrication approaches as outlined in Section I, are evaluated based on fabrication ease, considering factors such as cost, material and equipment requirements, and structural robustness. Notably, 3-D microfabrication techniques are advantageous due to their ability to realize complex microstructured geometries, using either impedance matching strategies or heterogeneous material compositions to improve absorption performance. While silicon-based absorbers are capable of covering millimeter-wave and terahertz frequency ranges and are generally cost-effective, their absorption performance remains limited to the 10–20-dB range. In contrast, resin-based absorbers fabricated via UV-cured micro 3-D printing have emerged as a highly promising alternative, offering significant advantages in cost-efficiency, mechanical robustness, and design adaptability over traditional methods [15]. Among the high-performance broadband absorber technologies, resin-based pyramidal absorbers uniquely surpass carbon-based polypropylene designs in terms of

structural durability, manufacturing flexibility, and customization potential. By leveraging resin micro 3-D printing, high-precision fabrication of microscale and flexible geometries becomes feasible, demonstrating versatility extending beyond instrumentation-centric use. For example, incorporation within enclosed metallic housings of high-frequency integrated systems enables effective suppression of interference due to in-package leakage, as well as suppression of undesired power in slab-mode dielectric devices [49]. Building on this capability, the present work introduces a general-purpose approach for realizing unconventional, fine-featured absorber structures tailored to diverse electromagnetic environments. The inherent manufacturing simplicity of integrating resin and liquid water unlocks a practical pathway toward broad applicability, enabling deployment across a wide range of application-specific scenarios requiring quasi-anechoic, broadband absorption up to 1000 GHz.

IV. Conclusion

We have proposed and experimentally validated a water-based broadband pyramid absorber up to 500 GHz. Using UV-cured resin 3-D printing, we have realized a microscale pyramidal array as a cost-effective and high-performance absorber suitable for compact terahertz systems beyond 1000 GHz, as demonstrated in simulations. The experimental results demonstrate absorption exceeding 99% across the entire band and 99.99% above 190 GHz up to 500 GHz. In addition, a theoretical analysis of the equivalent circuit model of the structure further confirms the observed impedance matching with free space. The results of full-wave simulation, equivalent-circuit modeling, and experimentation all show strong absorption in broadband, as well as consistent trends with respect to frequency. Overall, these results highlight the significant potential of resin micro 3-D printing for the realization of fine-featured, customizable shielding components tailored for next-generation 5G/6G wireless communication systems.

Acknowledgment

The authors would like to thank Jose Antonio Campo Santos for CNC machining, Ramzi Kattan for 3-D printing assistance, and Dr. Jessica Cesar Cuello for providing the WR-2.2 SGH antenna.

References

[1] H.-J. Song and N. Lee, "Terahertz communications: Challenges in the next decade," *IEEE Trans. THz Sci. Technol.*, vol. 12, no. 2, pp. 105–117, Mar. 2022.

[2] S. Nellen et al., "Coherent wireless link at 300 GHz with 160 Gbit/s enabled by a photonic transmitter," *J. Lightw. Technol.*, vol. 40, no. 13, pp. 4178–4185, Jul. 13, 2022.

[3] D. Headland, Y. Monnai, D. Abbott, C. Fumeaux, and W. Withayachumnankul, "Tutorial: Terahertz beamforming, from concepts to realizations," *APL Photon.*, vol. 3, no. 5, May 2018, Art. no. 051101.

[4] J. F. O'Hara, W. Withayachumnankul, and I. Al-Naib, "A review on thin-film sensing with terahertz waves," *J. Infr., Millim., THz Waves*, vol. 33, no. 3, pp. 245–291, Mar. 2012.

[5] L. Yi et al., "Towards practical terahertz imaging system with compact continuous wave transceiver," *J. Lightw. Technol.*, vol. 39, no. 24, pp. 7850–7861, Dec. 21, 2021.

[6] H. Sarieddeen, N. Saeed, T. Y. Al-Naffouri, and M.-S. Alouini, "Next generation terahertz communications: A rendezvous of sensing, imaging, and localization," *IEEE Commun. Mag.*, vol. 58, no. 5, pp. 69–75, May 2020.

[7] H. Lees, D. Headland, S. Murakami, M. Fujita, and W. Withayachumnankul, "Terahertz radar with all-dielectric leaky-wave antenna," *APL Photon.*, vol. 9, no. 3, Mar. 2024, Art. no. 036107.

[8] A. Masoomzadeh-Fard and S. Pasupathy, "Nonlinear equalization of multipath fading channels with noncoherent demodulation," *IEEE J. Sel. Areas Commun.*, vol. 14, no. 3, pp. 512–520, Apr. 1996.

[9] Z. Xu et al., "MIMO radar waveform design for multipath exploitation," *IEEE Trans. Signal Process.*, vol. 69, pp. 5359–5371, Oct. 2021.

[10] M. Amano and Y. Kotsuka, "A method of effective use of ferrite for microwave absorber," *IEEE Trans. Microw. Theory Techn.*, vol. 51, no. 1, pp. 238–245, Jan. 2003.

[11] K. Naishadham and P. K. Kadaba, "Measurement of the microwave conductivity of a polymeric material with potential applications in absorbers and shielding," *IEEE Trans. Microw. Theory Techn.*, vol. 39, no. 7, pp. 1158–1164, Jul. 1991.

[12] B.-K. Chung and H.-T. Chuah, "Modeling of RF absorber for application in the design of anechoic chamber," *Prog. Electromagn. Res.*, vol. 43, pp. 273–285, 2003.

[13] E&C Anechoic Chambers. *WAVASORBÂ VHP: Advanced Broadband Pyramidal Absorber*. Accessed: Mar. 20, 2025. [Online]. Available: https://www.ecanechoicchambers.com/pdf/WAVASORB

[14] A. Tamminen, A. Lonnqvist, J. Mallat, and A. V. Raisanen, "Monostatic reflectivity and transmittance of radar absorbing materials at 650 GHz," *IEEE Trans. Microw. Theory Techn.*, vol. 56, no. 3, pp. 632–637, Mar. 2008.

[15] J. Säily and A. V. Räisänen. (2003). *Studies on Specular and Non-specular Reflectivities of Radar Absorbing Materials (RAM) at Submillimetre Wavelengths*. THz Knowl. Inst. [Online]. Available: https://research.aalto.fi/en/publications/studies-on-specular-and-non-specular-reflectivities-of-radar-abso

[16] N. I. Landy, S. Sajuyigbe, J. J. Mock, D. R. Smith, and W. J. Padilla, "Perfect metamaterial absorber," *Phys. Rev. Lett.*, vol. 100, Jun. 2008, Art. no. 207402.

[17] W. Withayachumnankul and D. Abbott, "Metamaterials in the terahertz regime," *IEEE Photon. J.*, vol. 1, no. 2, pp. 99–118, Aug. 2009.

[18] E. Manikandan, S. S. Princy, B. S. Sreeja, and S. Radha, "Structure metallic surface for terahertz plasmonics," *Plasmonics*, vol. 14, no. 6, pp. 1311–1319, Dec. 2019.

[19] D. Yi, X.-C. Wei, and Y.-L. Xu, "Tunable microwave absorber based on patterned graphene," *IEEE Trans. Microw. Theory Techn.*, vol. 65, no. 8, pp. 2819–2826, Aug. 2017.

[20] E. S. Torabi, A. Fallahi, and A. Yahaghi, "Evolutionary optimization of graphene-metal metasurfaces for tunable broadband terahertz absorption," *IEEE Trans. Antennas Propag.*, vol. 65, no. 3, pp. 1464–1467, Mar. 2017.

[21] Z.-C. Lin, Y. Zhang, L. Li, Y.-T. Zhao, J. Chen, and K.-D. Xu, "Extremely wideband metamaterial absorber using spatial lossy transmission lines and resistively loaded high impedance surface," *IEEE Trans. Microw. Theory Techn.*, vol. 71, no. 8, pp. 3323–3332, Aug. 2023.

[22] M. Zdrojek et al., "Graphene-based plastic absorber for total sub-terahertz radiation shielding," *Nanoscale*, vol. 10, no. 28, pp. 13426–13431, 2018.

[23] R. Kakimi, M. Fujita, M. Nagai, M. Ashida, and T. Nagatsuma, "Capture of a terahertz wave in a photonic-crystal slab," *Nature Photon.*, vol. 8, no. 8, pp. 657–663, Aug. 2014.

[24] Y. Z. Cheng et al., "Ultrabroadband plasmonic absorber for terahertz waves," *Adv. Opt. Mater.*, vol. 3, no. 3, pp. 376–380, Mar. 2015.

[25] H. Liu, K. Luo, S. Tang, D. Peng, F. Hu, and L. Tu, "An ultra-wideband THz/IR metamaterial absorber based on doped silicon," *Materials*, vol. 11, no. 12, p. 2590, Dec. 2018.

[26] X. You et al., "Ultra-wideband far-infrared absorber based on anisotropically etched doped silicon," *Opt. Lett.*, vol. 45, no. 5, pp. 1196–1199, 2020.

[27] Y. Peng et al., "Ultra-broadband terahertz perfect absorber by exciting multi-order diffractions in a double-layered grating structure," *Opt. Exp.*, vol. 23, no. 3, pp. 2032–2039, 2015.

[28] Z. Shen, S. Li, Y. Xu, W. Yin, L. Zhang, and X. Chen, "Three-dimensional printed ultrabroadband terahertz metamaterial absorbers," *Phys. Rev. Appl.*, vol. 16, no. 1, Jul. 2021, Art. no. 014066.

[29] S. Li, Z. Shen, W. Yin, L. Zhang, and X. Chen, "3D printed cross-shaped terahertz metamaterials with single-band, multi-band and broadband absorption," *Opt. Mater.*, vol. 122, Dec. 2021, Art. no. 111739.

[30] T. Kubiczek, B. Sievert, D. Erni, and J. C. Balzer, "Broadband terahertz absorber from 3D-printed resin," in *Proc. 15th German Microw. Conf. (GeMiC)*, Duisburg, Germany, Mar. 2024, pp. 49–52, doi: 10.23919/gemic59120.2024.10485328.

[31] J. F. Federici, J. Ma, and L. Moeller, "Review of weather impact on outdoor terahertz wireless communication links," *Nano Commun. Netw.*, vol. 10, pp. 13–26, Dec. 2016.

[32] Q. Jin, E. Yiwen, K. Williams, J. Dai, and X.-C. Zhang, "Observation of broadband terahertz wave generation from liquid water," *Appl. Phys. Lett.*, vol. 111, no. 7, Aug. 2017, Art. no. 071103.

[33] Y. Lu, J. Chen, and J. Li, "Design of all-dielectric ultra-wideband transparent water-based absorber," *J. Phys. D, Appl. Phys.*, vol. 55, no. 11, Mar. 2022, Art. no. 115502.

[34] H. L. Phan et al., "High efficiency and ultra-wideband water-based microwave absorber using 3D printing," *Opt. Commun.*, vol. 556, Apr. 2024, Art. no. 130297.

[35] J. Ren and J. Yin, "Cylindrical-water-resonator-based ultra-broadband microwave absorber," *Opt. Mater. Exp.*, vol. 8, no. 8, pp. 2060–2071, 2018.

[36] J. Xie et al., "Truly all-dielectric ultrabroadband metamaterial absorber: Water-based and ground-free," *IEEE Antennas Wireless Propag. Lett.*, vol. 18, no. 3, pp. 536–540, Mar. 2019.

[37] J. Wen, Q. Ren, R. Peng, and Q. Zhao, "Multi-functional tunable ultra-broadband water-based metasurface absorber with high reconfigurability," *J. Phys. D, Appl. Phys.*, vol. 55, no. 28, Jul. 2022, Art. no. 285103.

[38] X. Zhang, F. Yan, X. Du, W. Wang, and M. Zhang, "Broadband water-based metamaterial absorber with wide angle and thermal stability," *AIP Adv.*, vol. 10, no. 5, May 2020, Art. no. 055211.

[39] J. Ge, Y. Zhang, H. Li, H. Dong, and L. Zhang, "Ultra-broadband, tunable, and transparent microwave meta-absorber using ITO and water substrate," *Adv. Opt. Mater.*, vol. 11, no. 10, May 2023, Art. no. 2202873.

[40] Y. Chen et al., "Ultrabroadband microwave absorber based on 3D water microchannels," *Photon. Res.*, vol. 9, no. 7, pp. 1391–1396, 2021.

[41] M. L. P. Bailey et al., "Narrow-band water-based absorber with high return loss for terahertz spectroscopy," *IEEE Trans. Terahertz Sci. Technol.*, vol. 5, no. 6, pp. 961–966, Nov. 2015.

[42] G. Ma et al., "A novel multilayer broadband terahertz metamaterial absorber based on three- dimensional printing and microfluidics technologies," *IEEE Trans. Terahertz Sci. Technol.*, vol. 14, no. 4, pp. 484–494, Jul. 2024.

[43] G. Deng et al., "Tunable terahertz metamaterial wideband absorber with liquid crystal," *Opt. Mater. Exp.*, vol. 11, no. 12, pp. 4026–4035, Dec. 2021.

[44] J. T. Kindt and C. A. Schmuttenmaer, "Far-infrared dielectric properties of polar liquids probed by femtosecond terahertz pulse spectroscopy," *J. Phys. Chem.*, vol. 100, no. 24, pp. 10373–10379, Jan. 1996.

[45] V. A. Markel, "Introduction to the Maxwell Garnett approximation: Tutorial," *J. Opt. Soc. Amer. A, Opt. Image Sci.*, vol. 33, no. 7, pp. 1244–1256, 2016.

[46] D. M. Pozar, *Microwave Engineering*, 4th ed., Hoboken, NJ, USA: Wiley, 2012.

[47] D. A. Frickey, "Conversions between S, Z, Y, H, ABCD, and T parameters which are valid for complex source and load impedances," *IEEE Trans. Microw. Theory Techn.*, vol. 42, no. 2, pp. 205–211, Feb. 1994.

[48] M. W. B. Silva and L. C. Kretly, "A new concept of RAM-radiation absorbent material: Applying corrugated surfaces to improve reflectivity," in *IEEE MTT-S Int. Microw. Symp. Dig.*, Natal, Brazil, Oct. 2011, pp. 556–560, doi: 10.1109/IMOC.2011.6169338.

[49] D. Headland, D. C. Gallego, M. Sakaki, N. Benson, and G. Carpintero, "Multi-octave all-dielectric directional coupler using integrated half-mirror for ultrawideband terahertz systems," *Laser Photon. Rev.*, p.2401644, 2025, doi: 10.1002/lpor.202401644.

[50] R. Wylde. *Space Qualified Tessellating TeraHertz RAMs for the 50 to 1000 GHz Region and Beyond*. Accessed: Nov. 18, 2024. [Online]. Available: https://www.terahertz.co.uk/